THE UNIVERSITY OF MICHIGAN

College of Engineering

Department of Mechanical Engineering

Cavitation and Multiphase Flow Laboratory

Report No. UMICH 03371-14-T

SPHERICAL DROPLET IMPINGEMENT ON FLAT RIGID SURFACE NON-SLIP BOUNDARY CONDITION

by

Yen C. Huang*

F. G. Hammitt**

Wen-Jei Yang***

Submitted to the Fourth Conference on Fluid Mechanics and Fluid Machinery
Budapest, Hungary

Financial Support Provided by:

National Science Foundation
Grant No. GK-730

* Former Research Associate and Doctoral Candidate
** Professor-In-Charge
*** Professor

SPHERICAL DROPLET IMPINGEMENT ON FLAT RIGID SURFACE: NON-SLIP BOUNDARY CONDITION

by

Huang, Y. C., Hammitt, F. G., Yang, Wen-Jei

USA

SUMMARY

The impact of spherical water drops upon a rigid non-slip plane is studied. The governing partial differential equations of compressible hydrodynamics neglecting body force, viscosity and surface tension are solved with a new Compressible-Cell-and-Marker numerical technique. Flow patterns, impact pressures, and velocities are found as a function of time. As the liquid boundary is free to deform, compression and rarefaction take place simultaneously after the first instant of impact. However, the net effect of compression is predominate during the early stages of impact, until the radial lateral flow velocity exceeds the impact velocity, after which the pressures attenuate. The maximum pressure attained for liquid impact Mach Numbers = 0.2 and 0.5 are about 60%* of the theoretical one-dimensional water-hammer pressure as corrected for changed sonic velocity. This latter point is of considerable importance in estimating damage capability of such impacts.

---

* The maximum pressures attained are about 80% and 120% of the conventional water hammer pressure $\rho_o C_o V_o$ for liquid impact Mach Numbers = 0.2 and 0.5 respectively.

NOMENCLATURE

Symbol	Description
A	Exponent in Tait's equation of state
B	Constant in Tait's equation of state
C	Shock wave velocity
C_o	Sonic Velocity
D	Diameter
H_1, H_2	Dimensions of Computation Domain in z- and r- direction, respectively
K	Constant
L	Length
M	Mach number
p	Pressure
p^o	$p/\rho_o C_o V_o$
R	Radius
R_m	Location of marker m in r- coordinate
r	Radial coordinate
r^o	r/R
t	Time
t^o	Non-dimensional time, Ct/D
U	Marker velocity component in z-direction
u	Velocity component in z-direction
u_n	Velocity component in normal direction
V	Marker velocity component in r-direction
v	Velocity component in r-direction
v_t	Velocity component in tangential direction
V_o	Impact velocity
x_n	Coordinate in normal direction
x_t	Coordinate in tangential direction

z	Vertical coordinate
z^o	z/L
Z_m	Location of marker m in z-coordinate
α	Stability factor
ρ	Density
Δ	Increment

Subscripts

c	Characteristic parameter
m	Marker index
n	Normal direction
o	Initial value
t	Tangential direction

Superscripts

o	Non-dimensional variable

LIST OF FIGURES

Figure		Page
1.	Shape-Time History of an Initially Spherical Droplet at Mach Number = 0.2 and 0.5 for Non-Slip Boundary Condition	11
2a-d	Isobar Distribution in an Initially Spherical Droplet at Time (Ct/D) = 0.125, 0.25, 1.0, and 2.5 respectively, at Impact Mach Number of 0.2 and 0.5 for Non-Slip Boundary Condition	12
3.	Pressure-Time History at Liquid-Solid Interface (z = 0) of an Initially Spherical Droplet at Impact Mach Number of 0.2 and 0.5 for Non-Slip Boundary Condition	16
4.	Pressure-Time History along the Symmetrical Axis (r =0) of an Initially Spherical Droplet at Impact Mach Number of 0.2 and 0.5 for Non-Slip Boundary Condition	17
5.	Pressure-Time History at Locations "a" (r = 0, z = 0.5L), "b" (r = 0, z = 0), "c" (r = 0.5R, z = 0) and "d" (r = 0.85R, z = 0) Spherical Droplet at Impact Mach Number of 0.2 and 0.5 for Non-Slip Boundary Condition	18
6.	Radial Velocity-Time History at Liquid-Solid Interface (r =0) of an Initially Spherical Droplet at Impact Mach Number of 0.2 and 0.5 for Non-Slip Boundary Condition	19
7.	Maximum Pressure Gradient-Time and Location Relation and Contact Edge-Time History of an Initially Spherical Droplet at Impact Mach Number of 0.2 and 0.5 for Non-Slip Boundary Condition	20

1. INTRODUCTION

Liquid droplet impingement is a serious and limiting phenomenon at the present time in various important technological fields such as large steam turbines, high-speed fixed-wing aircraft and helicopters, simply to name three of the most prominent. Also, applications involving cavitation should also be included due to the well recognized similarities between these forms of attack.

A useful and necessary approach to obtain quickly the engineering information necessary for the continued development of machinery elements such as these is the testing of candidate materials under droplet impingement attack in the laboratory. However, a long-range solution to the problem, allowing the eventual development of predicting ability, requires an analysis of both reaction of the material to a given imposed pressure-time distribution, and also of the detailed fluid-flow regime during the impact in order to obtain the pressure and velocity distributions on the surface as a function of time. For a "real" surface, i.e., one where some deformation occurs during the impact, the two problems are coupled. However, this is not the case if complete surface rigidity is assumed (material with infinite elastic modulus and strength, and infinite sonic velocity). Such an idealized material behaves at least approximately like many real materials during water droplet impact with air Mach Numbers of the order 1 to 2*, which is the range of interest for the technological applications previously mentioned. It is to this problem that the present analysis resulting from the doctoral dissertation of the first author[1] is addressed. The dissertation showed that the pressures and velocities during the earliest portion of the collision, which is also that of major importance since these quantities are maximized during this time, depend upon liquid impact Mach Number, droplet shape (spherical, cylindrical, combined spherical-cylindrical, a non-dimensional time parameter, etc.),

---

*The present study considers liquid Mach Numbers of 0.2 and 0.5 which are then equivalent.

and whether or not liquid slip was assumed at the solid interface.

Results with various combinations of the independent parameters have already been reported[2,3,4,5]. The present paper considers in particular the case of a spherical water drop impinging upon a flat, completely rigid, surface, where a non-slip boundary condition is assumed between the impinging liquid and the surface. Such a boundary condition is of course requisite with real fluids, and implies the existance of at least a small liquid viscosity. However, viscosity is not considered elsewhere in the analysis, and is not believed to be important for fluids such as cold water. Liquid compressibility is considered, as is necessary to obtain a meaningful solution.

The remarkable appearance of an impacting liquid drop has been observed for centuries, but detailed studies of the process were not possible until the development of high-speed photographic techniques. Worthington[6] gave the first extensive description around 1893. More recently the phenomenon has been investigated much more intensely. To name just a few of such studies: Edgerton and Killian[7] used droplet impingement to illustrate their photographic techniques: Hobbs and Kezweenz[8] studied the break-up of the rebounding drop. Engel[9] examined the dynamics of an impinging water sphere. Fyall[10] and many others, have been concerned with the damage process on a high speed vehicle by collision with raindrops in the atmosphere.

These previous investigations are primarily experimental. Fully theoretical analysis has been precluded by the formidable task of solving the pertinent non-linear partial differential equations. Harlow and Shannon[11] employed the Marker-and-Cell numerical method to obtain computer solutions of the full Navier-Stokes equations describing the flow dynamic during the splash for a viscous, incompressible fluid. Amsden[12] developed the Particle-in-Cell method for the calculation of the dynamics of compressible fluids, but this code is suitable only for hypervelocity impact where the target material behaves as a fluid also. For the response of a liquid drop at intermediate values of the impact liquid Mach Number, V_o/C_o,

an application of considerable technological importance, we have developed the Compressible-Cell-and-Marker numerical method herein described.

II. ANALYSIS

When a free spherical water drop collides with a rigid non-slip plane, the liquid is compressed, deformed and diverted into lateral flow. Equations and boundary conditions describing the situation are well known, but it is precluded to seek a closed form solution through a formidable and probably impossible analytical method. Our approach, therefore, has been numerical, using our newly-developed Compressible-Cell-and-Marker (ComCAM) technique to obtain computer solutions of simplified Navier-Stokes equations for an inviscid, compressible fluid. The purpose is to determine the flow dynamics during the impact and thereby to explain some of the experimental results that have been published with little or no correlative interpretation.

The governing equations in cylindrical coordinates with axial symmetry for a spherical water drop are

$$\frac{\partial \rho}{\partial t} + \frac{\partial (\rho u)}{\partial z} + \frac{1}{r}\frac{\partial (r\rho v)}{\partial r} = 0 \tag{1}$$

$$\frac{\partial (\rho u)}{\partial t} + \frac{\partial (\rho u^2)}{\partial z} + \frac{1}{r}\frac{\partial (r\rho uv)}{\partial r} = -\frac{\partial p}{\partial z} \tag{2}$$

$$\frac{\partial (\rho v)}{\partial t} + \frac{\partial (\rho vu)}{\partial z} + \frac{1}{r}\frac{\partial (r\rho v^2)}{\partial r} = -\frac{\partial p}{\partial r} \tag{3}$$

The quasi-steady states are assumed and the density ρ and the pressure p are coupled by the equation of state for water

$$\frac{p + B}{p_o + B} = \left(\frac{\rho}{\rho_o}\right)^A$$

which was first proposed by Tait[13]. The proper values of the two constants for cold water are as reported by Cole[14].

$$A = 7.15 \text{ and } B = 3008 \text{ atm}$$

The above set of equations (1) through (4) are used to find impact pressure and velocity distribution within the liquid boundary. Since the boundary is free to move, it is necessary to keep track of its location by

imbedding marker particles on the boundary. This arrangement is possible because of the condition that fluid particles initially on the free boundary always remain on the free boundary, as argued by Lamb[15].

The appropriate equations for the marker particles used to indicate the interface movements are

$$\frac{d(\rho U)}{dt} = -\frac{dp}{dz} \tag{5}$$

$$\frac{d(\rho V)}{dt} = -\frac{dp}{dr} \tag{6}$$

$$Z_m = \int U dt \tag{7}$$

$$R_m = \int V dt \tag{8}$$

where U and V are the marker velocity components, Z_m and R_m are marker locations in z- and r- coordinates respectively.

The appropriate initial conditions over the domain of calculation are

$$p = p_o \qquad u = u_o \qquad v = v_o$$

where p_o is the environmental pressure, u_o and v_o are the initial impact velocities in the z- and r- direction respectively. In the case of a normal impact (i.e., perpendicular), $v_o = 0$ and $V_o = u_o$

The appropriate boundary conditions are:

i) along the axis of symmetry (z), r=0, and symmetry requires

$$v = 0, \quad \frac{\partial u}{\partial r} = 0, \quad \frac{\partial p}{\partial r} = 0$$

ii) along the impacted rigid surface, z = 0, v = 0, u = 0, $\frac{\partial p}{\partial z} = 0$, for non-slip wall condition

iii) along the free surface, the incompressible continuity condition yields

$$p = p_o, \quad \frac{\partial u_n}{\partial x_n} = \frac{\partial v_t}{\partial x_t} = 0$$

where u_n and v_t are the moving velocity components of the liquid air interface in the normal x_n and tangential x_t directions of the surface respectively.

iv) along the sides of the finite computational domain, permeable boundary conditions will be imposed, in such a way that the normal

space derivative of the variable vanishes at the boundary,

$$\frac{\partial u}{\partial z} = 0, \quad \frac{\partial v}{\partial z} = 0, \quad \frac{\partial p}{\partial z} = 0 \text{ at } z = H_1$$

$$\frac{\partial u}{\partial r} = 0, \quad \frac{\partial v}{\partial r} = 0, \quad \frac{\partial p}{\partial r} = 0 \text{ at } r = H_2$$

where H_1 and H_2 are sizes of computational domain in the z- and r- direction, respectively.

All the above equations are then nondimensionalized and approximated by finite difference expressions corresponding to the mesh of computational cells over the domain. The initial-value problems are solved by advancing the configuration through a set of finite time steps or computational cycles. Each numerical computational cycle consists of the following steps .

1) Marker particles on the fluid boundary are moved to appropriate new positions.
2) The continuity and momentum equations are used to advance the densities and velocities through the time change of one cycle by an explicit technique.
3) The pressure is calculated as a function of densities according to the equation of state, assuming quasi-steady process.
4) Boundary condition values and time counters are adjusted to prepare the next computational cycle.

The results are printed periodically including the configuration of marker particles, the pressures, velocities and momentums.

The numerical results represent approximate solutions to the original differential equations, since derivatives are replaced by finite differences. Terms of the order of the square of the time increment and spatial step size are neglected. The convergence of the finite difference representation, i.e., the degree to which the approximate solution approaches the exact solution, must then be examined.

It is known that although the explicit formulation avoids the need of iterative or matrix inversion techniques, the Courant stability criterion must be satisfied, i.e., the distance a wave travels in the time increment

Δz or Δr. That is:

$$\Delta t < \frac{\text{min. } (\Delta z, \Delta r)}{C} \tag{9}$$

where C is the shock wave velocity in the liquid phase. With the definition of the stability factor

$$\alpha = \frac{C\,\Delta t}{\text{min. } (\Delta z, \Delta r)}$$

one can satisfy the stability criterion by selecting a value of α less than unity.

Numerical experiments were carried out to determine the stability factor and required numbers of cells so that convergence of the result is reasonably assured, in regard to magnitudes, timing, and wave shapes. For actual study, a stability factor $\alpha = 0.1$ and 20 x 40 mesh were used.

The detailed description of the ComCAM method was given by Huang[1].

III. RESULTS AND DISCUSSION

In examining the results for two impact Mach numbers of 0.2 and 0.5, one must consider the following. Constant atmospheric pressure at the water-air free surface is imposed. The impact plane is perfectly rigid, flat, but non-slippery. The water is assumed inviscid, without surface tension, but compressible and elastic. The fracture strength of water is taken to be 270 atm., an experimental result of Brigg[16]. Of course, ordinarily impure water will rupture at much smaller tensions, but perhaps not for the very short duration of tension here involved. The two constants in Tait's equation of state for water are A = 7.15 and B = 3008 atm.

Fig. 1 shows the deformation of an initially spherical droplet at various time instants following an impact on a rigid plane at Mach Numbers = 0.2 and 0.5 for non-slip boundary condition. The upper half of the droplet remains relatively undeformed up to the time of $t^o = 1$, while the deformation near the contact edge is not apparent at least up to $t^o = 0.25$

Fig. 2a through 2d show the isobar distribution at various instants. The major pressure release comes mostly from the radial flow along the impacted surface and less from the rebound on the top of the drop. While

the liquid - solid interface acts like a pressure source, the liquid-air free surface serves as a pressure sink. These two effects interfuse with each other. The exact consequence depend upon both location and time.

Fig. 3 shows the pressure distribution on the impacted surface ($z = 0$) at various time instants. From these curves, one can see that the time-rate change of pressure as well as the spatial pressure gradient are greater near the contact edge than those at the center (0, 0) of the contact area during the period dominated by compression.

Fig. 4 shows the pressure distribution on the axis of symmetry ($r = 0$) at several time instants. By comparing the curves at times 0.25 and 0.5, one can see that while the pressures on the upper portion continue to increase, the pressure near the rigid plane ($z = 0$) start to fall. As the effect of rarefaction propagates from the stagnation point toward the top of the droplet, the pressure diminishes everywhere toward the stagnation pressure along the axis of symmetry.

Fig. 5 shows the pressure at four given locations as a function of time. The pressure at the stagnation point "a" reaches its peak value at time $t^o = 0.2$, and then subsides to about the final steady-state stagnation pressure. The pressure at a location on the axis of symmetry ($r = 0$, $z = 0.5R$) behaves in a similar manner except with a time lag. Since this location lies between the stagnation point and the top of the droplet, it is credible that this pressure-time curve lies below the pressure-time curve for the stagnation point. The pressures at "c" and "d" on the impacted surface remains unaffected until the contact ring reaches that point. The time-rate of change in pressure for rising portion of the curve "c" and "d" is about the same as that of the curve "a" for the stagnation point. The pressure at "c" rises and at some time exceeds the respective pressure at the stagnation point "a", before it starts to fall along with the latter.

Fig. 6 shows the radial velocity distribution on the impacted surface ($z = 0$). The dotted lines signify the portion of the liquid which is very close to, but not actually in contact with, the impacted plane ($z = 0$). The velocity and the location indicated by the end of a dotted line are those which photographic observations of the impacted droplet would indicate

(Fig. 8 from reference 9). The maximum radial velocity at any given instant occurs at a location between the tip of jetting and the center line (r = 0). For an impact liquid Mach Number of 0.2, the absolute maximum radial velocity is 2.65 times the impacting velocity V_o in the case of a free-slip boundary condition, which has been reported elsewhere [3], and 2.86 times V_o in the present case of a non-slip boundary condition. These calculations are in good agreement with the experimental results of Fyall [10]. He used the technique of high speed photography and observed that the radial velocity during the first three microseconds was 3056 ft/sec for an impact speed of 990 ft/sec with a 2mm waterdrop. Perspex was used as a target material in his case.

The present calculations indicate that the lateral flow and pressure build-up begins simultaneously with impact, but that jetting is not appreciable during the early stage of impact, (Fig. 1 and 2). The pressure is highest at the center of the contact area and decreases to atmospheric pressure at the edge, where it is just about to be contacted by the rigid plane. Due to the presence of this radial pressure gradient, the liquid flows radially to expand the contact area. The radial velocity at the contact edge is often decelerated by the liquid rushing toward the rigid plane. However, the protrusion in the contact periphery is so slight that it is almost impossible to detect or measure by experiments or photographical means. The fact that compression and rarefaction take place simultaneously from the very beginning of impact is strictly in accordance with the governing equations. Thus it is only an approximation that would assume no gross flow or splashing at the very beginning of impact. Since the boundary condition of atmospheric pressure on the contact edge should be satisfied at all times, the pressure is released by the lateral flow from the first instant of contact, and hence, the impact pressure becomes less than the theoretical one-dimensional maximum pressure, as depicted in Figs. 3, 4, and 5.

Fig. 7 shows the magnitude and location of the maximum radial pressure gradient on the impacted surface. The higher the impact Mach

number, the greater the peak of pressure gradient. It is conjectured that the material may be damaged by this severe pressure gradient.

Fig. 8 illustrates photographs taken from Engel[9], of the deformation stages for a water droplet following an impact on a solid plane. This experimental evidence of the physical process is very much in agreement with the analytical results calculated in this paper (Fig. 1).

IV. CONCLUSIONS

The objective of this paper was to study the hydrodynamic phenomena during the impact of a spherical liquid drop on a rigid plane. Effort was directed to investigate the effect of the spherical curvature of the drop. Pressure and velocity distributions were found as a function of time. The following conclusions can be drawn.

1. The impact is characterized entirely by liquid impact Mach Number and non-dimensional time in this case. In general, it is a function of these independent parameters and droplet shape and surface effects (as liquid slip).

2. Since the liquid surface is free to deform, the pressure build-up is affected by the immediate radial release flow from the first instant of impact.

3. From the first instant of contact, the compression and rarefaction effects are superimposed at the same point for a spherical drop. Consequently, the maximum pressure generated in a spherical drop is lower than that in a finite cylindrical jet of the same radius (as shown in ref. 5). In both cases the pressure is well less than the theoretical one-dimensional pressure.

4. Since the maximum radial pressure gradient on the impact surface is greater in the case of a spherical drop than in the case of a finite cylindrical jet, the maximum radial lateral flow velocity is greater for the spherical drop than for the finite cylindrical jet. Therefore, the erosion caused by shear with this lateral flow, and its collisions with surface roughnesses, etc., may be higher for the spherical drop than for the cylindrical.

5. As was expected, the non-slip boundary condition retards the flow. However, it also contributes to a build-up in pressure inside the droplet. Accordingly, the instantaneous peak radial velocity is higher than for the free-slip case (as discussed in ref. 3). Otherwise, the patterns of pressure and velocity responses for the non-slip and free-slip cases are essentially analogous.

6. Unlike the impact of a cylindrical droplet (ref. 2 and 5) and the impact of a spherical-cylindrical composite droplet (ref. 4), there is no cavitation indicated in a spherical drop for the liquid impact Mach Numbers 0.2 and 0.5 investigated.

V. ACKNOWLEDGEMENT

The work was supported by National Science Foundation Grant No. GK 730.

Huang, Y.C.
Former Research Associate and Doctoral Candidate
Hammitt, F. G.
Professor-In-Charge
Yang, Wen-Jei, Professor
Department of Mechanical Engineering
312 Auto Laboratory, N. Campus
University of Michigan
Ann Arbor, Michigan 48105

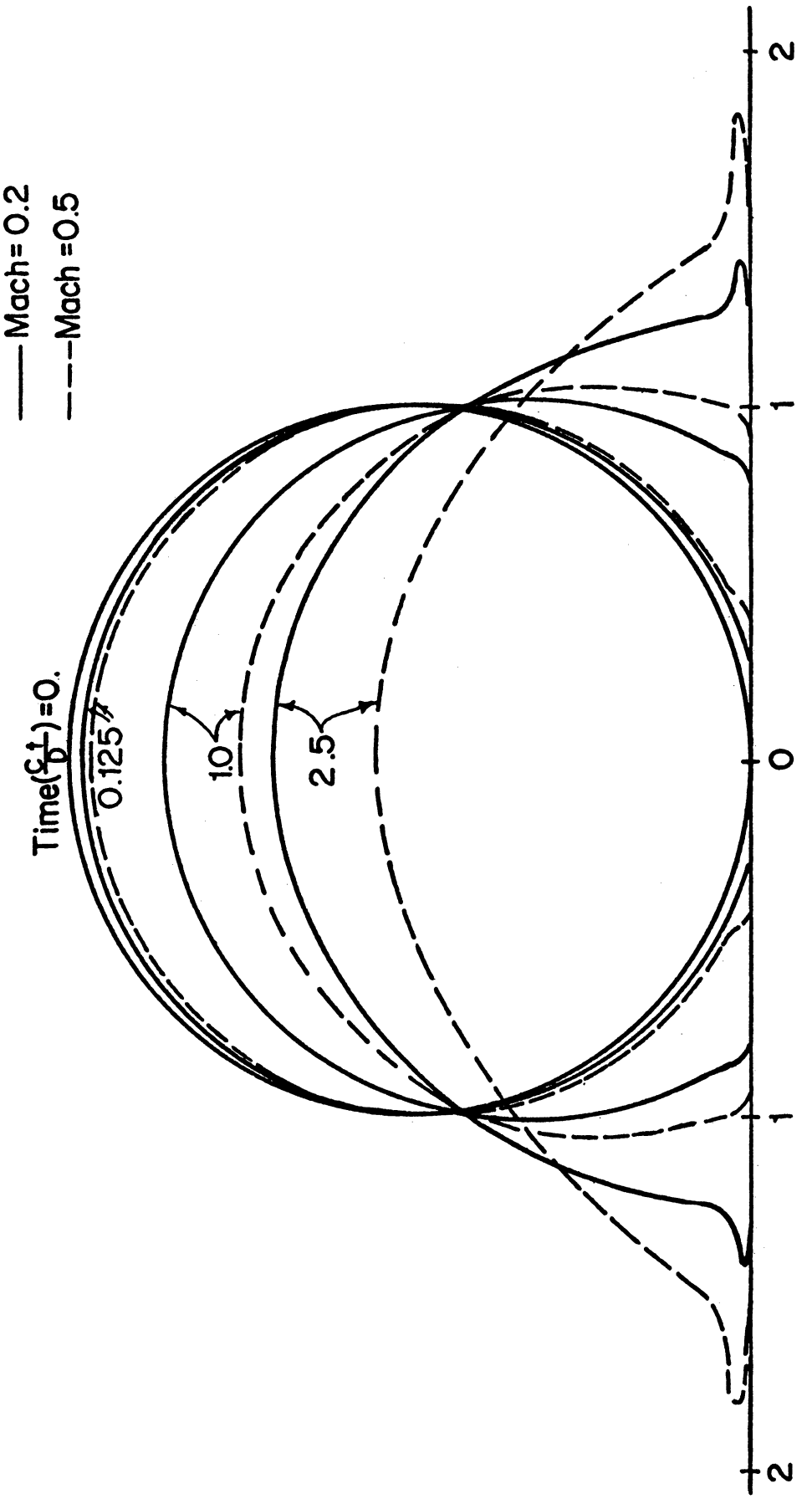

Fig. 1. Shape-Time History of an Initially Spherical Droplet at Mach Numbers = 0.2 and 0.5, for Non-Slip Boundary Condition

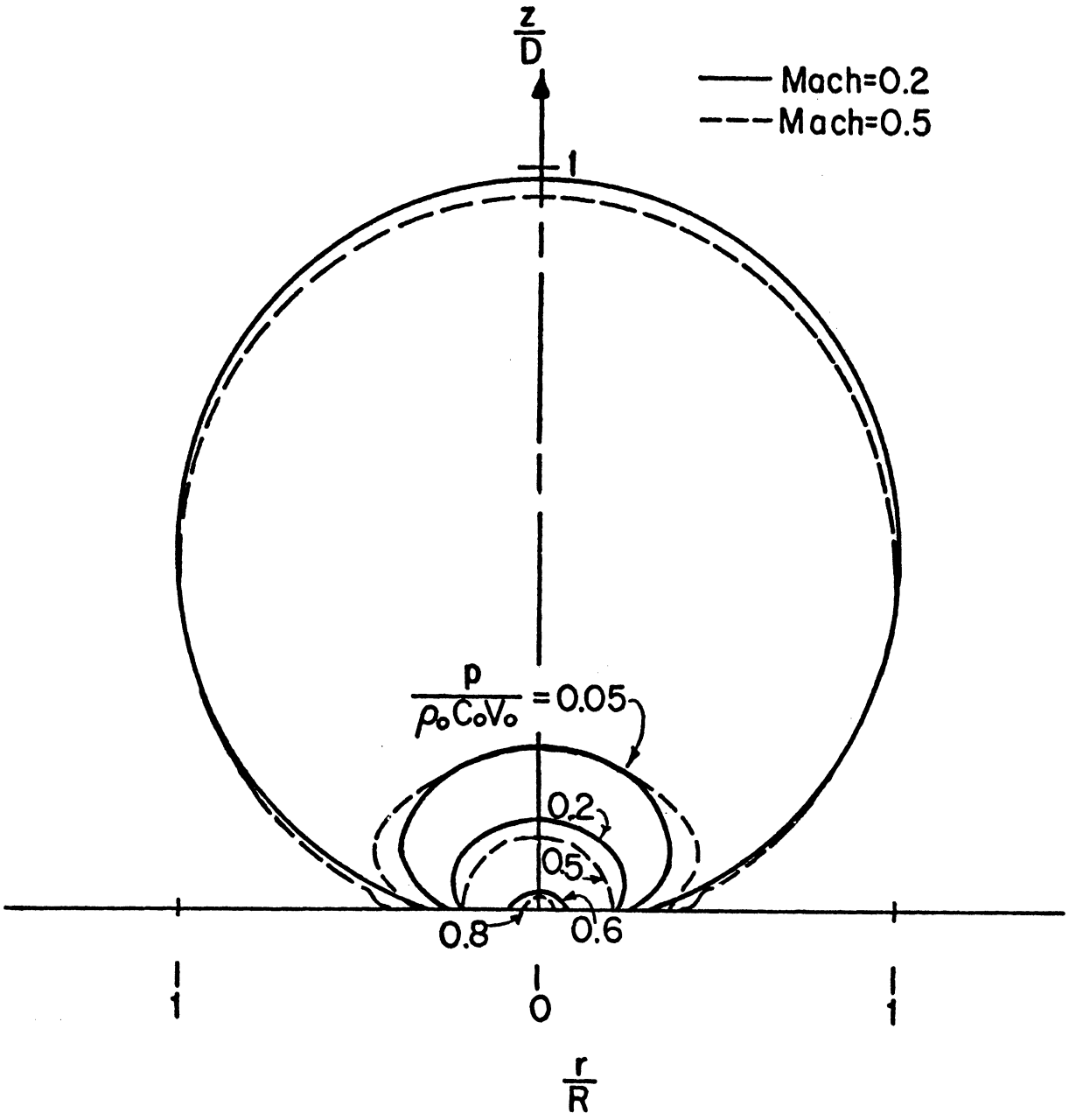

Fig. 2a. Isobar Distribution in an Initially Spherical Droplet at Time (Ct/D) = 0.125, for Impact Mach Numbers of 0.2 and 0.5. Non-Slip Boundary Condition.

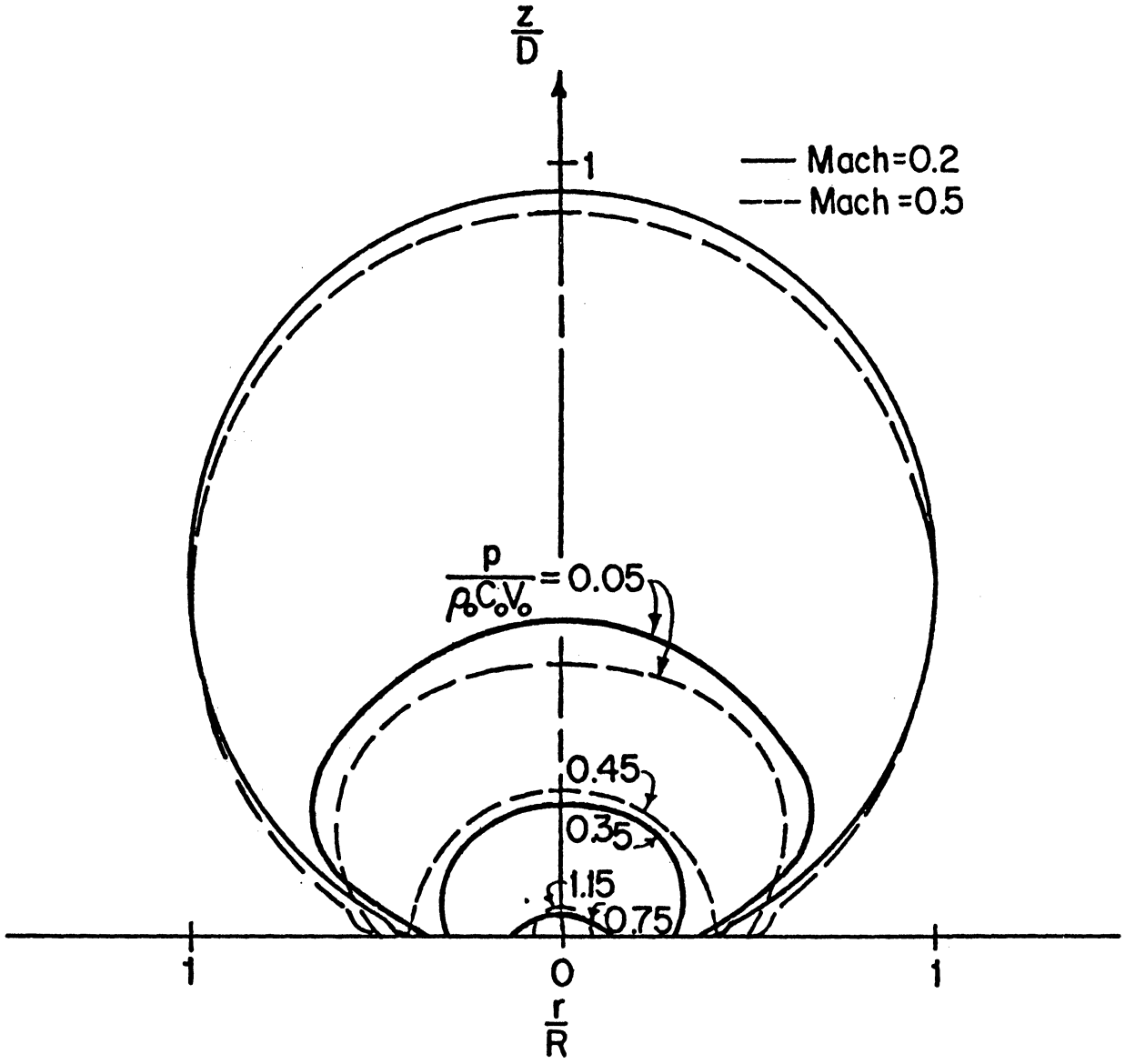

Fig. 2b. Isobar Distribution in an Initially Spherical Droplet at Time (Ct/D) = 0.25, for Impact Mach Numbers of 0.2 and 0.5. Non-Slip Boundary Condition.

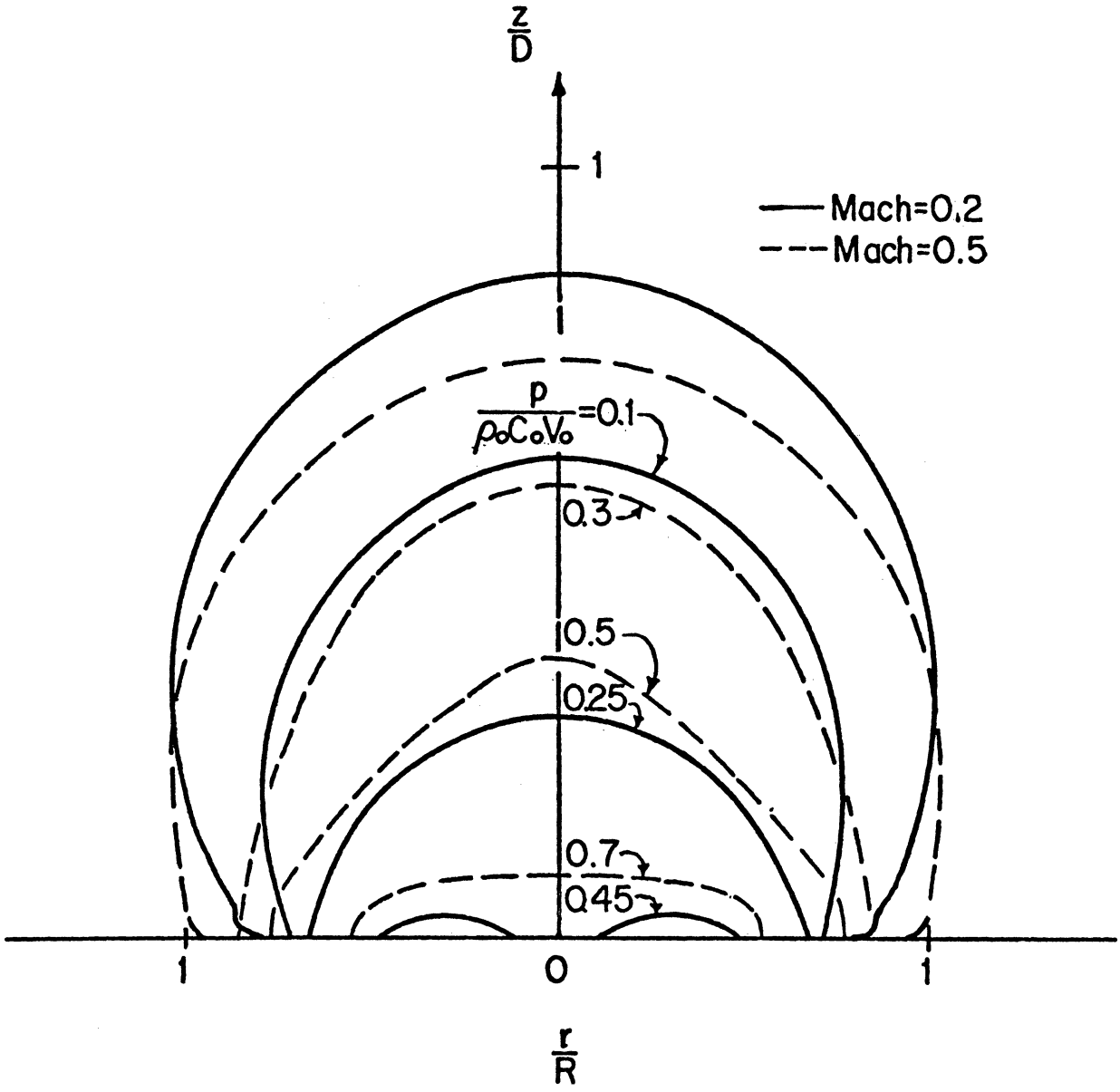

Fig. 2c. Isobar Distribution in an Initially Spherical Droplet at Time (Ct/D) = 1, for Impact Mach Numbers of 0.2 and 0.5. Non-Slip Boundary Condition.

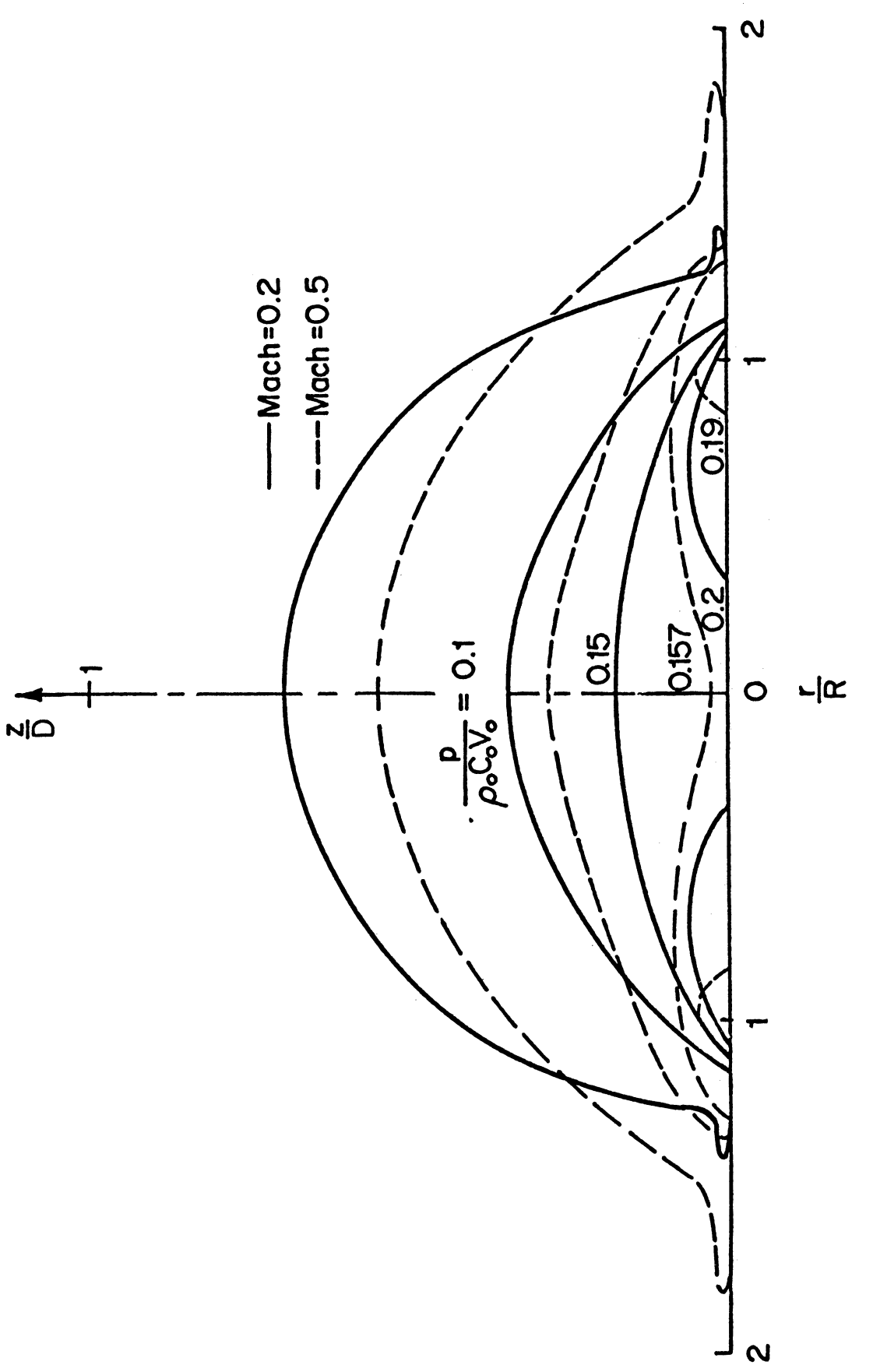

Fig. 2d. Isobar Distribution in an Initially Spherical Droplet at Time (Ct/D) = 2.5, for Impact Mach Numbers of 0.2 and 0.5. Non-Slip Boundary Condition.

Huang, Hammitt and Yang

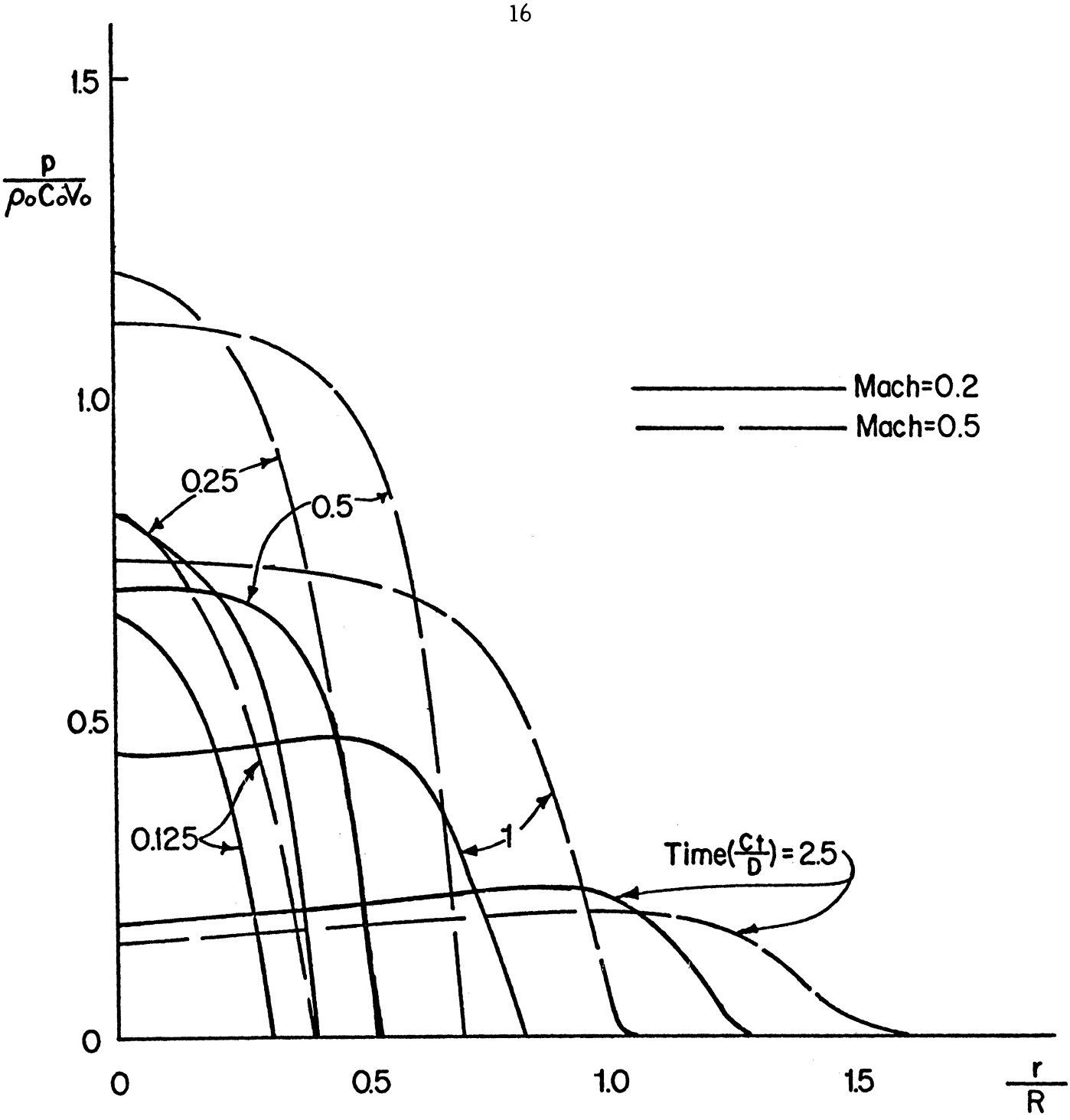

Fig. 3. Pressure-Time History at Liquid-Solid Interface (z = 0) of an Initially Spherical Droplet for Impact Mach Numbers of 0.2 and 0.5. Non-Slip Boundary Condition.

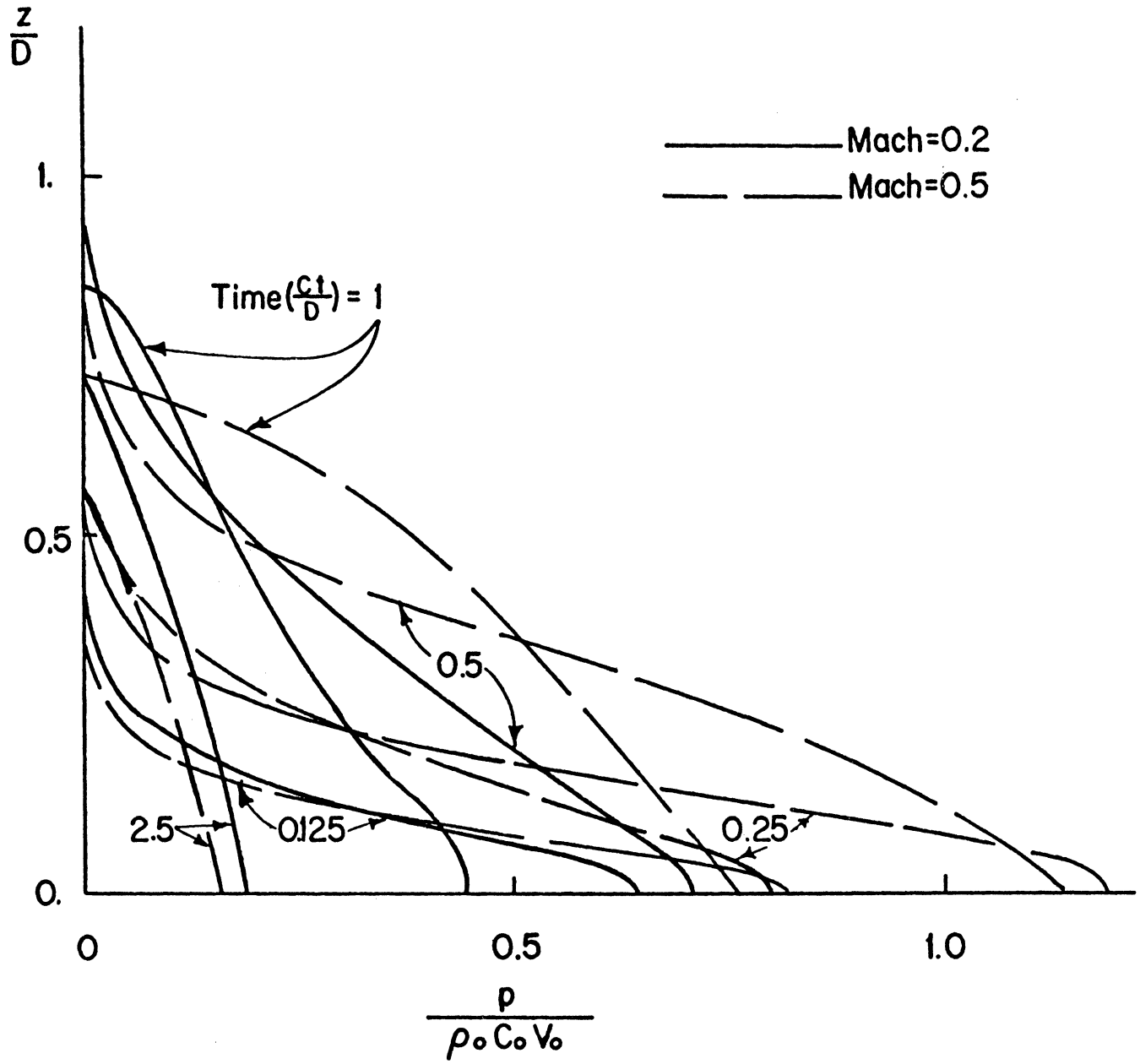

Fig. 4. Pressure-Time History along the Symmetrical Axis (r = 0) of an Initially Spherical Droplet for Impact Mach Numbers of 0.2 and 0.5. Non-Slip Boundary Condition.

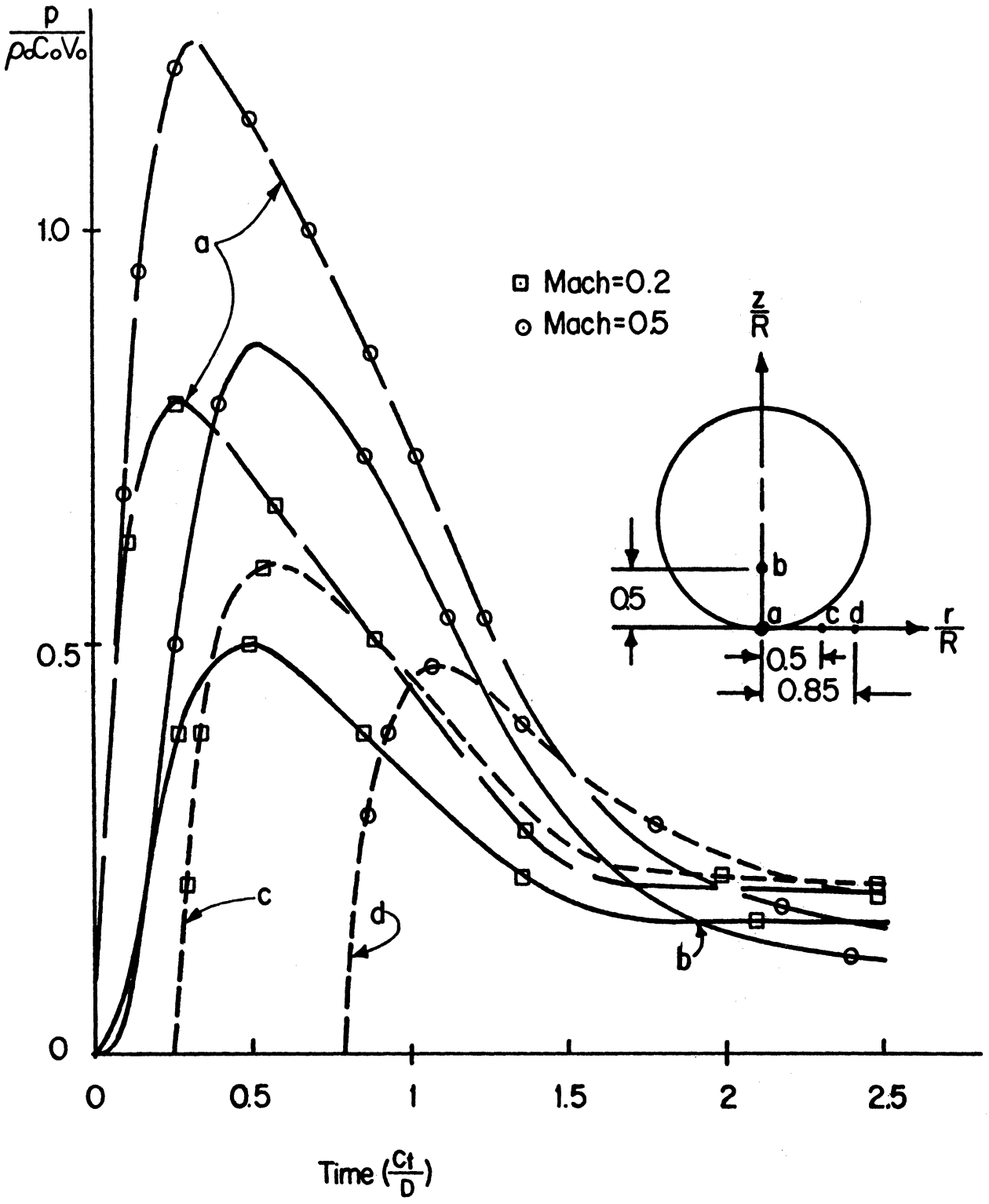

Fig. 5. Local Pressure-Time History in an Initially Spherical Droplet for Impact Mach Numbers of 0.2 and 0.5 and under Non-Slip Boundary Condition.

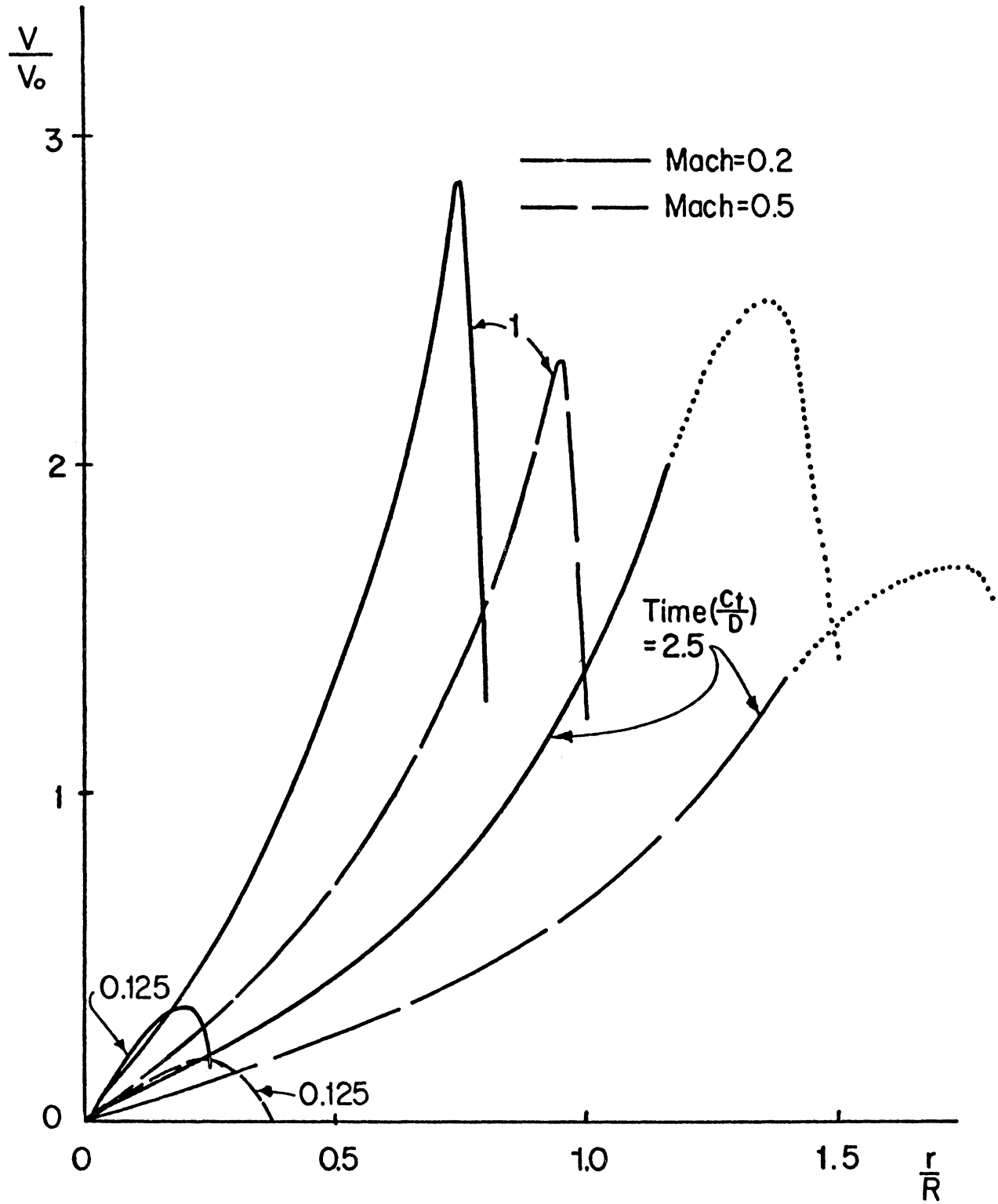

Fig. 6. Radial Velocity-Time History at Liquid-Solid Interface (r = 0) of an Initially Spherical Droplet for Impact Mach Numbers of 0.2 and 0.5. Non-Slip Boundary Condition.

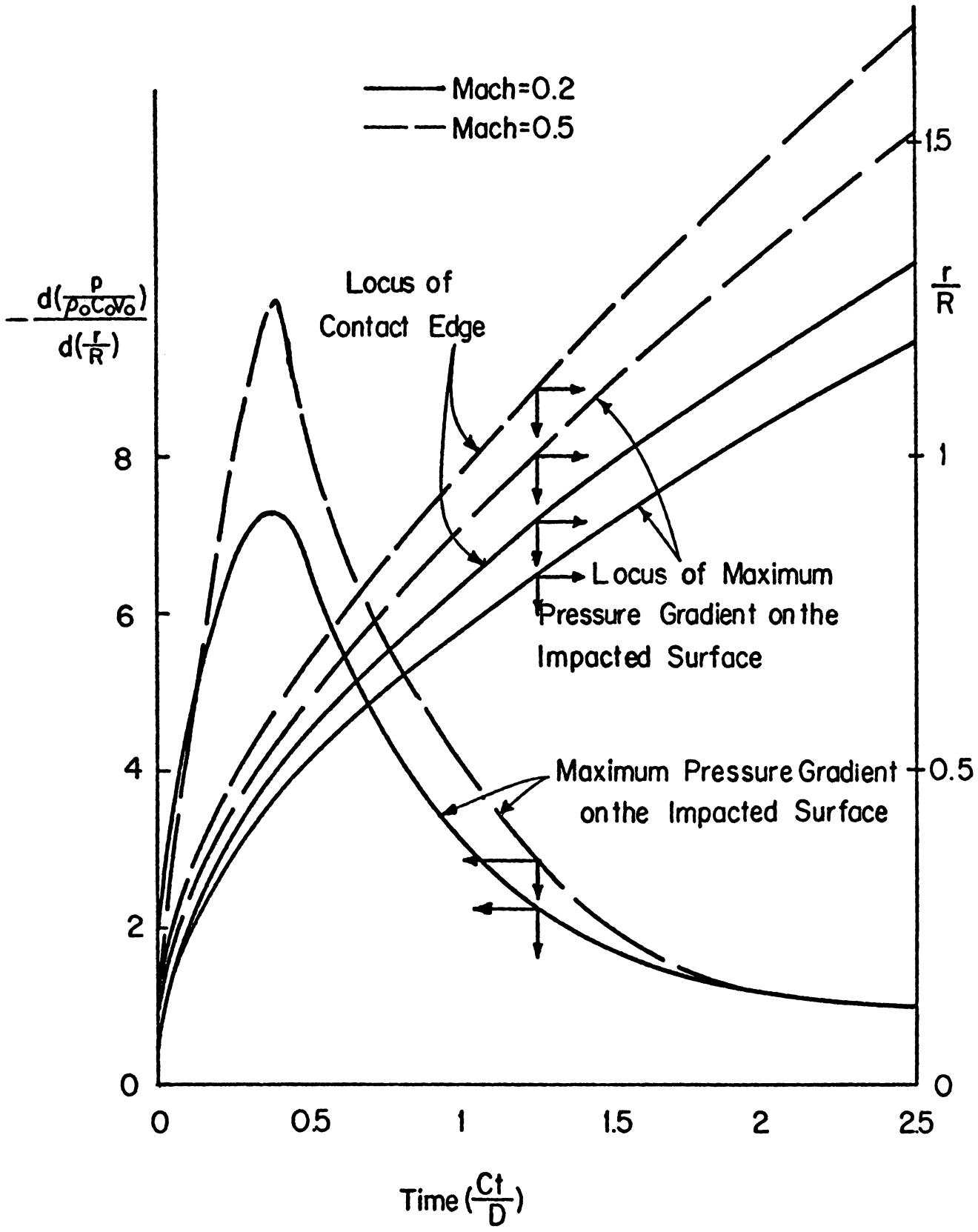

Fig. 7. Maximum Pressure Gradient-Time and -Location Relation and Contact Edge-Time History of an Initially Spheri-Droplet for Impact Mach Numbers of 0.2 and 0.5. Non-Slip Boundary Condition.

VI REFERENCES

1. Huang, Y. C.: Numerical Studies of Unsteady, Two-Dimensional Liquid Impact Phenomena. Ph.D. Thesis, University of Michigan. (1971)

2. Huang, Y. C., Hammitt, F. G. and Yang, Wen-Jei: Normal Impact Phenomena of a Finite Cylindrical Jet. Report No. UMICH 03371-9-T, University of Michigan. (1971)

3. Huang, Y.C., Hammitt, F.G. and Yang, Wen-Jei: Impact of Spherical Water Drop on Flat Rigid Surface. Report No. UMICH 03371-10-T, University of Michigan. (1971)

4. Huang, Y.C., Hammitt, F.G. and Yang, Wen-Jei: Computer Simulation of High Speed Collision with Rain Drop (Combined Spherical-Cylindrical Shape). Report No. UMICH 03371-12-T, University of Michigan. (1971)

5. Huang, Y.C., Hammitt, F.G. and Yang, Wen-Jei: Mathematical Modelling of Normal Impact Between a Finite Cylindrical Liquid Jet and Non-Slip Flat Rigid Surface. Report No. UMICH 03371-13-T, University of Michigan. (1971)

6. Worthington, A.M.: A Study of Splashes, The MacMillan Company, N.Y. . (1963)

7. Edgerton, H.E., and Killian, J.R., Jr.: Flash, Charles T. Bradford, Boston. (1954)

8. Hobbs, P.V., and Kezweeny, A.J.: Science, 155, p. 1112. (1967)

9. Engel, O.G.: Waterdrop Collisions with Solid Surfaces. J. of Research of the National Brueau of Standards, Vol. 54, No. 5, pp. 281-298. (1955)

10. Fyall, A.A.: Single Impact Studies of Rain Erosion. Shell Aviation News, Vol. 374, pp. 16-23. (1969)

11. Harlow, R.H. and Shannon, J. P.: The Splash of a Liquid Drop. J. of Applied Physics, Vol. 38, No. 10, pp. 3855-3866. (1967)

12. Amsden, A.A.: The Particle-in-Cell Method for the Calculation of the Dynamics of Compressible Fluids. Los Alamos Scientific Laboratory, Vol. LA. 3466. (1966)

13. Tait, P.G.: Report on Some of the Physical Properties of Fresh Water and Sea Water. Physical Chemistry, Vol. 2, pp. 1-71. (1888)

14. Cole, R.H.: Underwater Explosions. Dover Press. (1965)

15. Lamb, H.: Hydrodynamics, 6th Edition, Dover Press. (1965)

16. Briggs, L.J.: Limiting Negative Pressure of Water. J. of Applied Physics, Vol. 21, pp. 721-722. (1950)